

# Room temperature multiferroism in $\text{CaTcO}_3$ by interface engineering

Hongwei Wang,<sup>1,2</sup> Lixin He\*,<sup>1</sup> and Xifan Wu\*<sup>2</sup>

<sup>1</sup>*Key Laboratory of Quantum Information, University of Science and Technology of China, Hefei, Anhui, 230026, People's Republic of China*

<sup>2</sup>*Department of Physics, Temple University, Philadelphia, PA 19122, USA*

(Dated: June 7, 2018)

The structural instabilities of  $\text{ATcO}_3$  ( $A = \text{Ca, Sr, Ba}$ ) are investigated by first-principles calculations. In addition to the large octahedral rotation instability, a weak ferroelectric tendency is identified in  $\text{CaTcO}_3$ . We show that the ferroelectricity in  $\text{CaTcO}_3$  can be recovered by interface engineering based on  $\text{CaTcO}_3/\text{BaTcO}_3$  superlattices, where the octahedral rotation is largely suppressed. The Néel temperature is found to be  $\sim 816$  K, indicating that  $\text{CaTcO}_3$  can be engineered into a new room temperature multiferroic material.

PACS numbers: 77.55.Nv, 75.70.Cn, 77.80.bn

$\text{ABO}_3$  perovskite continues to prove itself to be an important family of multifunctional materials. This is because various instabilities can be simultaneously present within its simple cubic structure at high temperature [1–5]. Many of these instabilities such as magnetic, ferroelectric, antiferrodistortive, and antiferroelectric orderings and their interactions are closely associated with different functionalities that are useful for the device applications. Recently a lot of excitement has been generated, again, in  $\text{ATcO}_3$  ( $A = \text{Ca, Sr, Ba}$ ) as a new family of perovskite [6–8]. Similar to its isovalent neighbor of  $\text{Mn}(4s^23d^5)$ , technetium has a  $5s^24d^5$  electronic configuration with a completely occupied  $t_{2g}$  and completely empty  $e_g$  bands according to the crystal field theory under cubic symmetry. In the crystalline phase,  $\text{ATcO}_3$  is paraelectric and adopts a G-type antiferromagnetic (AFM) configuration as expected. Strikingly,  $\text{ATcO}_3$  is discovered to have an anomalously high magnetic ordering temperature, e.g.  $T_N \sim 800$  K in  $\text{CaTcO}_3$  [6–8]. This is in sharp contrast to that of manganese perovskite, in which  $\text{CaMnO}_3$  only has a Néel temperature of 123 K [9, 10]. Keeping this intriguing property in mind, one might be wondering whether more functionalities could be explored in this new family of perovskite?

In this work, we first use density functional theory (DFT) to perform an investigation of the structural instabilities in  $\text{ATcO}_3$ . An unexpected hidden ferroelectric (FE) instability is discovered in  $\text{CaTcO}_3$ , along with a much stronger antiferrodistortive (AFD) one in its cubic phase at high temperature. Based on a recently introduced interface engineering mechanism [11], we carry out DFT calculations in  $\text{CaTcO}_3/\text{BaTcO}_3$  supercells and explicitly show that the FE polarization can be recovered in interfacial layer, where the AFD instability associated with oxygen octahedral rotation is largely suppressed. The Néel temperature of the supercell is identified to be  $\sim 816$  K by a following Monte Carlo simulation. Our theoretical predictions clearly suggest that the room temperature multiferroism can be achieved in  $\text{CaTcO}_3$  by interface engineering.

Our DFT calculations are done by using the VASP code package [12, 13]. In particular, both hybrid DFT

within the Heyd-Scuseria-Ernzerhof (HSE) scheme [14] and the Perdew-Burke-Ernzerhof functional revised for solids (PBEsol) [15] functional are adopted to approximately treat the exchange correlation of electrons [16]. These DFT functionals are known to be very accurate in predicting the volume of solids which is particularly important because the FE instability is sensitive to the cell volume. The lattice constants are fully relaxed in bulk studies and allowed to relaxed in the [001] direction in  $\text{CaTcO}_3/\text{BaTcO}_3$  supercells, assuming an epitaxial growth on the substrate of  $\text{GdScO}_3$ .

Although the detailed experimental study of the structural phase transition is only available for  $\text{SrTcO}_3$  [8] and  $\text{CaTcO}_3$  [6]. It is generally accepted that  $\text{ATcO}_3$  share a common orthorhombic  $\text{Pnma}$  symmetry at low temperature and cubic  $\text{Pm}\bar{3}\text{m}$  symmetry at high temperature. In Table I, we present the computed structural parameters, in which a direct comparison is also made with experiments of the low temperature phase. Overall, it can be seen that PBEsol functional gives a very accurately prediction of lattice constants and volume, except that the lattice constant  $a$  is slightly overestimated by  $\sim 0.7\%$ . The HSE functional gives even better agreement with the experimental values. In the low temperature orthorhombic structure, the  $\text{TcO}_6$  octahedral is allowed to both rotate and tilt. It is interesting to note that with the increasing radius of  $A$  site atom, the rotational and tilting angles are decreasing from very large angle in  $\text{CaTcO}_3$  to almost zero in  $\text{BaTcO}_3$ . This trend is very similar to that of  $\text{ATiO}_3$ , which can be explained in terms of the so-called Goldschmidt tolerance factor [18], in which a small (large) tolerance factor favors (resists) octahedral rotation.

The oxygen rotation in both  $\text{CaTcO}_3$  and  $\text{SrTcO}_3$  indicates that there is a structural instability located at Brillouin zone boundary in their high temperature cubic phase. However, it will be also interesting to check whether there is any additional instabilities that might lead to functional properties. To this end, we perform the phonon band structure calculations along high symmetry points in the cubic phase of  $\text{ATcO}_3$  by HSE hybrid functional. As expected, we find that there is

TABLE I: Computed structural parameters, magnetic exchange angles ( $^\circ$ ), oxygen octahedral rotation  $\phi_r$  ( $^\circ$ ) and tilting angles  $\phi_t$  ( $^\circ$ ) of bulk ATcO<sub>3</sub> (A=Ca,Sr,Ba) with  $Pnma$  symmetry. The structural parameter, Born effective charges  $Z^*$ , and electronic contribution to dielectric constant  $\epsilon_\infty$  are also reported for Pm $\bar{3}m$  symmetry. Experimental values [7] are shown in parenthesis.

		CaTcO <sub>3</sub>	SrTcO <sub>3</sub>	BaTcO <sub>3</sub>
Pnma (HSE)	$a$ ( $\text{\AA}$ )	5.53 (5.53)	5.56 (5.54)	5.69
	$b$ ( $\text{\AA}$ )	7.71 (7.70)	7.86 (7.85)	8.05
	$c$ ( $\text{\AA}$ )	5.39 (5.39)	5.61 (5.58)	5.67
	$V$ ( $\text{\AA}^3$ )	230.05(229.15)	244.92 (242.74)	260.20
	$Tc - \bar{O}_1 - Tc$	150.90(150.43)	163.39 (161.57)	179.96
	$Tc - \bar{O}_2 - Tc$	150.91(151.53)	167.76 (166.96)	179.90
	$\phi_r$	10.04	0.60	0.049
	$\phi_t$	14.55	8.32	0.019
Pnma (PBEsol +U)	$a$ ( $\text{\AA}$ )	5.57 (5.53)	5.59 (5.54)	5.71
	$b$ ( $\text{\AA}$ )	7.73 (7.70)	7.90 (7.85)	8.08
	$c$ ( $\text{\AA}$ )	5.41 (5.39)	5.60 (5.58)	5.71
	$V$ ( $\text{\AA}^3$ )	232.08(229.15)	247.51 (242.74)	262.87
	$Tc - \bar{O}_1 - Tc$	148.41(150.43)	161.13 (161.57)	179.94
	$Tc - \bar{O}_2 - Tc$	148.91(151.53)	161.24 (166.96)	179.88
	$\phi_r$	10.63	6.18	0.058
	$\phi_t$	15.80	9.13	0.032
Pm $\bar{3}m$ (PBEsol +U)	$a$ ( $\text{\AA}$ )	3.93	3.97	4.03
	$Z_A^*$	2.69	2.66	2.87
	$Z_{Tc}^*$	5.87	5.96	6.19
	$Z_{O\parallel}^*$	-1.62	-1.62	-1.72
	$Z_{O\perp}^*$	-5.32	-5.38	-5.61
	$\epsilon_\infty$	8.64	8.60	9.14

no unstable phonon in BaTcO<sub>3</sub>, and an unstable AFD phonon at  $R$  point of Brillouin zone boundary in SrTcO<sub>3</sub> ( $\omega = 150i$   $\text{cm}^{-1}$ ), which becomes much more unstable in CaTcO<sub>3</sub> ( $\omega = 232.67i$   $\text{cm}^{-1}$ ). Surprisingly, we also identify a hidden FE phonon mode in CaTcO<sub>3</sub> at zone center ( $\omega = 58.82i$   $\text{cm}^{-1}$ ), however, weaker than that of the AFD mode as shown in Fig. 1. This suggests that cubic CaTcO<sub>3</sub> has a tendency to develop nonzero spontaneous polarization. In order to elucidate the nature of FE, we further compute the Born effective charge [19] and the results are shown in Table. 1. One can clearly see anomalously large effective charges on Tc and O<sub>||</sub>, which are similarly identified in conventional ferroelectrics such as BaTiO<sub>3</sub>. This suggest that the covalent bonding between Tc and oxygen atoms lies at the origin of the weak FE in CaTcO<sub>3</sub>, in which a large dynamic charge transfer results in a polar instability for the atomic displacement along the Tc-O bond direction [20]. Unfortunately, the ferroelectric tendency does not result in a condensation of FE ordering in its low temperature orthorhombic phase below 800 K, where CaTcO<sub>3</sub> stays paraelectric. This is due to the competition between the FE and AFD instabilities [21]. As a result, the development of ferroelectric polarization is prohibited in the presence of a strong tendency of oxygen octahedral rotation. With the intriguingly high Neél temperature, it is particularly desirable that the FE ordering could be recovered and turned into

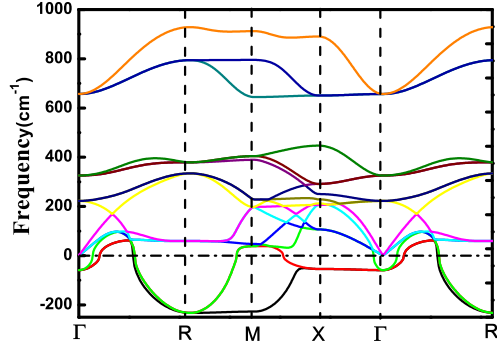


FIG. 1: (Color online) Phonon dispersions of the G-type AFM CaTcO<sub>3</sub> of Pm $\bar{3}m$  symmetry along the high-symmetry points, which are computed by HSE functional.

a new room temperature multiferroic material. However, additional material engineering is required.

The above can be achieved in the artificial materials of superlattices under epitaxial growth. In general, there are two kinds of approaches that can be used which are the *epitaxial strain* and *interface engineering* methods respectively. We first try the epitaxial method. To do so, we apply both tensile and compressive strain on the cubic CaTcO<sub>3</sub> systematically in the range of  $\pm \sim 5\%$ . At the same time, we lower the space group symmetry in the calculations to allow the development of polarization along both  $c$  axis and in the  $ab$  plane. For the epitaxial strain, the FE ordering usually has a much larger dependence on the strain through the strain polarization coupling than that of AFD ordering associated with oxygen rotation. It is expected that at certain strain, the ordering of AFD and FE can be switched. However our calculations show that CaTcO<sub>3</sub> persists to be paraelectric even as much as  $\pm 5\%$  has been applied.

We then focus on the possibility of interface engineering as the second option. Compared with epitaxial strain, more dramatic change in the strength of instabilities can be obtained at the interface resulting in an overall change of functionalities. In particular, it has been recently shown that a substantial reducing AFD mode at the interface layer of CaTiO<sub>3</sub>/BaTiO<sub>3</sub> can be used to enhance the FE [22]. Thus it will be very interesting to check if FE can be recovered in the CaTcO<sub>3</sub>/BaTcO<sub>3</sub> short-period superlattices. We carry out first-principles calculations for BaTcO<sub>3</sub>/CaTcO<sub>3</sub> superlattices assuming the coherent growth on the substrate of GdScO<sub>3</sub> ( $a = 3.97\text{\AA}$ ) [17]. This selection of substrate only introduces a small lattice mismatch by about  $\pm 1.26\%$  in BaTcO<sub>3</sub> and CaTcO<sub>3</sub>, which facilitates the experimental growth. The main results are shown in Table. II. As one of the most exciting results, the 1BaTcO<sub>3</sub>/1CaTcO<sub>3</sub> superlattice does exhibit a FE ordering with a spontaneous polarization  $P_s = 6.34$   $\mu\text{C}/\text{cm}^2$  along the [110] in-plane axis!

The emergence of FE ordering only in superlattice suggests that it is an interface effect. In order to further

elucidate its interfacial origin, we employ the layer polarization decomposition to analyze the local polarization profile [19]. The results are shown in Table. II along with the local oxygen octahedral rotation profile. Compared with the bulk  $\text{CaTcO}_3$ , it can be seen that both oxygen rotation and tilting angles associated with AFD are greatly reduced at the interfaces. As a result of the reduced AFD mode, we see the development of local polar distortion at the interfaces. Very interestingly, the local polar distortion is developed both along [110] and [001] directions. However, in the [001] direction the local polarization adopts an antiferroelectric-like profile and the resulting total polarization is almost zero. The interface nature of the induced FE can be more easily seen in the local polarization profile in  $2\text{BaTcO}_3/2\text{CaTcO}_3$  supercell. This is because both interface, bulk  $\text{BaTcO}_3$ , and bulk  $\text{CaTcO}_3$  layers can be found in 2:2 supercell. As a result, the local polarization of interface layers can be directly compared to those of bulks. The resulting local polarization profile is also presented in Table. II. Clearly, it can be seen that the polar distortions are only developed at the interfaces along both [110] and [001] directions. This is due to the interface suppression of AFD similar to what has been already seen in 1:1 supercell. However, as soon as the bulk  $\text{BaTcO}_3$  or  $\text{CaTcO}_3$  layer is reached, the local polarization disappears immediately. At the same time both oxygen octahedral rotation and tilting angles recover to the bulk magnitudes. This is consistent with the complete absence of FE instability in  $\text{BaTcO}_3$  and the dominant AFD instability over FE in  $\text{CaTcO}_3$ . We want to stress that the FE will be only induced in the  $\text{CaTcO}_3$  layer when the oxygen rotation is suppressed which lies at the heart of our interface design.

TABLE II: Layer-by-layer decompositions of polarization  $p(\mu\text{C}/\text{cm}^2)$ , oxygen octahedral rotation  $\phi_r(^{\circ})$ , and tilting  $\phi_t(^{\circ})$  in the supercells of  $1\text{BaTcO}_3/1\text{CaTcO}_3$  (1BT1CT) and  $2\text{BaTcO}_3/2\text{CaTcO}_3$  (2BT2CT), which are computed by PBEsol+U functional.

		CT	Interface	BT	Interface
1BT1CT	$p_{[110]}$	-	6.31	-	6.18
	$p_{[001]}$	-	1.53	-	-1.59
	$\phi_r$	-	5.82	-	5.94
	$\phi_t$	-	12.76	-	6.05
2BT2CT	$p_{[110]}$	0.15	9.42	-0.072	-9.06
	$p_{[001]}$	0.045	1.56	0.058	-1.56
	$\phi_r$	9.76	5.97	0.46	5.77
	$\phi_t$	14.63	9.52	4.40	9.50

Both  $\text{BaTcO}_3$  and  $\text{CaTcO}_3$  have been found to have high Neél temperature well above room temperature. It has been argued that the more delocalized  $4d$  or-

bitally enhance the covalent hybridization with neighboring oxygen atoms, which in turn increase the hopping matrix according to the Anderson-Goodenough-Kanamori rules [6, 23]. Therefore, it can be expected that the large magnetic antiferromagnetic coupling will be kept in the  $\text{BaTcO}_3/\text{CaTcO}_3$  superlattices. To further confirm this, we map the total energies in different magnetic configurations onto the Heisenberg Hamiltonian [4]. The exchange coupling constants include the nearest-neighbor ( $J^1$ ) and next-nearest-neighbor ( $J^2$ ), beyond which the coupling constant is found to be very small and could be neglected. This coupling constants are further decomposed into the contributions from intralayer ( $J_{\text{intra}}$ ) and interlayers ( $J_{\text{inter}}$ ). The results are listed in Table III. One can see that the exchange coupling constants are approximately the averages of those of the bulk  $\text{BaTcO}_3$  and bulk  $\text{CaTcO}_3$  in both intra- and inter-layer contributions. We obtain the AFM phase transition at 816 K from the Monte Carlo simulation.

TABLE III: Magnetic moments  $m(\mu_B)$ , exchange coupling constants  $J(\text{meV})$ , and Neél temperature  $T_N(\text{K})$  of bulk  $\text{CaTcO}_3$ , bulk  $\text{BaTcO}_3$ , and  $1\text{CaTcO}_3/1\text{BaTcO}_3$  supercell. PBEsol+U functional is used in the DFT calculations.

	$\text{CaTcO}_3$	$\text{BaTcO}_3$	$1\text{CaTcO}_3/1\text{BaTcO}_3$
$m$	2.14	2.09	2.05
$J_{\text{inter}}^1$	-38.10	-69.02	-52.60
$J_{\text{intra}}^1$	-38.10	-69.02	-60.29
$J_{\text{inter}}^2$	-0.78	-1.09	-2.89
$J_{\text{intra}}^2$	-0.78	-1.09	-3.17
$T_N$	602	1089	816

In conclusion, a hidden ferroelectric instability is identified in  $\text{CaTcO}_3$ , however suppressed by the large oxygen octahedral rotation. We use the first-principles calculations to show that the polarization can be induced by an interface engineering method in the proposed  $\text{BaTcO}_3/\text{CaTcO}_3$  superlattices. Our computational results confirm the room temperature multiferroism in the superlattice.

LH acknowledges the support from the Chinese National Fundamental Research Program 2011CB921200 and National Natural Science Funds for Distinguished Young Scholars. XW acknowledges the financial support of start-up fund of Temple University and computational support by the National Science Foundation through TerraGrid resources provided by NICS under grant number [TG-DMR120045].

\* To whom correspondence should be addressed: helx@ustc.edu.cn, xifanwu@temple.edu.

[1] H. Y. Hwang, Y. Iwasa, M. Kawasaki, B. Keimer, N. Nagaosa, and Y. Tokura, Nat. Mater. **11**, 103 (2012).

[2] J. Hong and D. Vanderbilt, Phys. Rev. B **87**, 064104 (2013)

- [3] J. W. Bennett, K. F. Garrity, K. M. Rabe, and D. Vanderbilt, Phys. Rev. Lett. **110**, 017603 (2013).
- [4] J. H. Lee and K. M. Rabe, Phys. Rev. B **84**, 104440 (2011).
- [5] J. H. Lee and K. M. Rabe, Phys. Rev. Lett. **107**, 067601 (2011).
- [6] M. Avdeev, G. J. Thorogood, M. L. Carter, B. J. Kennedy, J. Ting, D. J. Singh, and K. S. Wallwork, J. Am. Chem. Soc. **133**, 1654 (2011).
- [7] C. Franchini, T. Archer, J. He, X. Chen, A. Filippetti, and S. Sanvito, Phys. Rev. B **83**, 220402 (2011).
- [8] E. E. Rodriguez, F. Poineau, A. Llobet, B. J. Kennedy, M. Avdeev, G. J. Thorogood, M. L. Carter, R. Seshadri, D. J. Singh, and Anthony K. Cheetham, Phys. Rev. Lett. **106**, 067201 (2011).
- [9] H. Taguchi, Phys. Stat. Sol. **88**, K79 (1985).
- [10] T. Günter, E. Bousquet, A. David, Ph. Boullay, Ph. Ghosez, W. Prellier, and M. Fiebig, Phys. Rev. B **85**, 214120 (2012).
- [11] H. Wang, L. He, and X. Wu, Europhys. Lett. **100**, 17005 (2012).
- [12] G. Kresse and J. Hafner, Phys. Rev. B **47**, R558 (1993).
- [13] G. Kresse and J. Furthmüller, Phys. Rev. B **54**, 11169 (1996).
- [14] J. Heyd, G. E. Scuseria, and M. Ernzerhof, J. Chem. Phys. **118**, 8207 (2003).
- [15] J. P. Perdew, A. Ruzsinszky, G. I. Csonka, O. A. Vydrov, G. E. Scuseria, L. A. Constantin, X. L. Zhou, and K. Burke, Phys. Rev. Lett. **100**, 136406 (2008).
- [16] In the calculation based on PBEsol functional, an on-site Coulomb interaction term  $U = 3.0$  eV and exchange interaction  $J = 1$  eV are used for technetium. In our HSE hybrid functional calculations, a mixing parameter of  $a = 0.3$  is adopted. A 500 eV plane-wave energy cutoff and  $6 \times 6 \times 4$   $k$  mesh points converge very well the results. Ionic coordinates are considered to be fully relaxed until the Hellmann-Feynman force is less than  $1$  meV/Å.
- [17] *Physics of Ferroelectrics: A Modern Perspective*, edited by K. M. Rabe, C. H. Ahn, and J.-M. Triscone, Springer, Berlin (2007).
- [18] V. M. Goldschmidt, Die Gesetze der Krystallochemie, Die Naturwissenschaften, **21**, 477 (1926).
- [19] X. Wu, O. Diéguez, K. M. Rabe, and D. Vanderbilt, Phys. Rev. Lett. **97**, 107602 (2006).
- [20] R. E. Cohen and H. Krakauer, Phys. Rev. B **42**, 6416 (1990).
- [21] W. Zhong and D. Vanderbilt, Phys. Rev. Lett., **74**, 2587 (1995).
- [22] X. Wu, K. M. Rabe, and D. Vanderbilt, Phys. Rev. B, **83**, 020104 (2011).
- [23] J. B. Goodenough, *Magnetism and the chemical bond* (John Wiley and Sons, New York-London, 1993)